
JOSIAH WILLARD GIBBS
BORN FEB. 11, 1839—DIED APR. 28, 1903


John Gamble Kirkwood
1907 — 1959
Physical Chemist
S.B.–University of Chicago (1926)
Ph.D.–Massachusetts Institute of Technology
(1929): Sc.D. (Honoris Causa)–University
of Chicago (1954) and Universite Libre d
Bruxelles (1959)
Served: Yale University as Sterling
Professor of Chemistry: Chairman of the
Chemistry Department (1951 — 1959) and
Director of Division of Sciences (1956 —
1959): Leiden University as Lorentz Professor
of Theoretical Physics (1959): California
Institute of Technology as Noyes Professo
of Chemistry (1947 – 1951): Cornell University
as Todd Professor of Chemistry (1938 – 1947):
National Academy of Sciences as Foreign
Secretary (1954 – 1958); The United States
Government as Scientific Consultant (1941-1959)
Scientific Honors: American Chemical
Society Award in Pure Chemistry (1936):
Richards Medal (1950): Lewis Medal (1955)
LARS ONSAGER
1903 — 1976
BORN OSLO, NORWAY
L WILLARD GIBBS PROFESSOR
NOBEL LAUREATE *
ARGARETHE ONSAGER
1912 — 1991
N MARBURG, AUSTRIA
*ETC
CAMBRIDGE
UNIVERSITY

2006 Summer School on Computational Materials Science

Lecture Notes: Ab Initio Molecular Dynamics Simulation Methods in Chemistry

Victor S. Batista*

Yale University, Department of Chemistry, P.O.Box 208107, New Haven, Connecticut 06520-8107, U.S.A.

I Introduction

These lectures will introduce computational methods that provide quantum mechanical descriptions of the dynamical and equilibrium properties of polyatomic systems.[1–7] According to the fifth postulate of quantum mechanics, the description of dynamics requires solving the time-dependent Schrödinger equation

$$i\frac{\partial \Psi_t(x)}{\partial t} = \hat{H}\Psi_t(x), \tag{1}$$

subject to a given initial condition, $\Psi_0(x)$. To keep the notation as simple as possible, all expressions are written in atomic units, so $\hbar = 1$. Here, $\hat{H} = \hat{p}^2/(2m) + V(\hat{x})$ is the Hamiltonian operator, $\hat{p} = -i\nabla$ is the momentum operator and $V(\hat{x})$ is the potential energy operator. A formal solution of Eq. (1) can be obtained by integration, as follows:

$$\Psi_t(x) = \int dx' \langle x|e^{-i\hat{H}t}|x'\rangle\langle x'|\Psi_0\rangle, \tag{2}$$

where the Kernel $\langle x|e^{-i\hat{H}t}|x'\rangle$ is the quantum propagator.

As an example, consider a diatomic molecule vibrating near its equilibrium position $\bar{x}$ where the potential is Harmonic,

$$V(\hat{x}) = \frac{1}{2}m\omega^2(\hat{x} - \bar{x})^2. \tag{3}$$

The description of the time-dependent bond-length $x(t)$ is given by the expectation value

$$x(t) = \langle \Psi_t|\hat{x}|\Psi_t\rangle, \tag{4}$$

where Ψ_t is defined according to Eq. (2) with the particular Kernel,

$$\langle x|e^{-i\hat{H}t}|x'\rangle = \sqrt{\frac{m\omega}{2\pi \mathsf{sinh}(it\omega)}}\mathsf{exp}\left(-\frac{m\omega}{2\mathsf{sinh}(\omega it)}[(x^2 + x'^2)\mathsf{cosh}(\omega it) - 2xx']\right). \tag{5}$$

This standard formulation of quantum mechanics relies upon the tools of *calculus* (*e.g.*, derivatives, integrals, etc.) and involves equations and operations with infinitesimal quantities as well as states in Hilbert-space (the infinite dimensional space of functions L^2). These equations, however, seldom can be solved analytically as shown in the example above. Therefore, computational solutions are necessary. However, computers can not handle infinite spaces since they have only limited memory. In fact, all they *can* do is to store and manipulate discrete arrays of numbers. Therefore, the question is: how can we represent continuum states and operators in the space of memory of digital computers?

*E-mail: victor.batista@yale.edu

II Grid-Based Representations

In order to introduce the concept of a grid-representation, we consider the state,

$$\Psi_0(x) = \left(\frac{\alpha}{\pi}\right)^{1/4} e^{-\frac{\alpha}{2}(x-x_0)^2 + ip_0(x-x_0)}, \tag{6}$$

which can be expanded in the infinite basis set of delta functions $\delta(x-x')$ as follows,

$$\Psi_0(x) = \int dx' c(x') \delta(x-x'), \tag{7}$$

where $c(x') \equiv \langle x'|\Psi_0\rangle = \Psi_0(x')$.

A grid-based representation of $\Psi_0(x)$ can be obtained, in the coordinate range $x = (x_{min}, x_{max})$, by discretizing Eq. (7) as follows,

$$\Psi_0(x) = \Delta \sum_{j=1}^{n} c_j \delta(x-x_j), \tag{8}$$

where the array of numbers $c_j \equiv \langle x_j|\Psi_0\rangle$ represent the state Ψ_0 on a grid of equally spaced coordinates $x_j = x_{min} + (j-1)\Delta$ with finite resolution $\Delta = (x_{max} - x_{min})/(n-1)$.

Note that the grid-based representation, introduced by Eq. (8), can be trivially generalized to a grid-based representation in the multidimensional space of parameters (*e.g.*, x_j, p_j, γ_j, ... etc.) when expanding the target state $\Psi_0(x)$ as a linear combination of basis functions $\langle x|x_j, p_j, \gamma_j\rangle$, with expansion coefficients as $c_j \equiv \langle x_j, p_j, \gamma_j|\Psi_0\rangle$.

Problem 1: Write a Fortran code to represent the wave-packet, introduced by Eq. (6) on a grid. Visualize it with Gnuplot. Choose $x_0 = 0$ and $p_0 = 0$, in the range x=(-20,20), with $\alpha = \omega m$, where $m = 1$ and $\omega = 1$. If this is your first Fortran code, copy the attached solution into a file named Problem1.f, compile it by typing f77 Problem1.f -o Problem1, run it by typing ./Problem1, and visualize the output by first typing gnuplot, and then typing plot "arch.0000". Type quit, to exit Gnuplot.

Next, we consider grid-based representations in momentum space:

$$\Psi_0(p) = \langle p|\Psi_0\rangle. \tag{9}$$

Inserting the closure relation $\hat{1} = \int dx|x\rangle\langle x|$ in Eq. (9), we obtain that

$$\langle p|\Psi_0\rangle = \int dx \langle p|x\rangle\langle x|\Psi_0\rangle = (2\pi)^{-1/2} \int dx e^{-ipx} \langle x|\Psi_0\rangle. \tag{10}$$

is the Fourier transform of the initial state since

$$\langle p|x\rangle = (2\pi)^{-1/2} e^{-ip\hat{x}}. \tag{11}$$

The Fourier transform can be efficiently implemented in $O(N\log(N))$ steps, when $\langle x|\Psi_0\rangle$ is represented on a grid with $N = 2^n$ points (where n is an integer), by using the Fast Fourier Transform (FFT) algorithm.[8] In contrast, the implementation of the Fourier transform by quadrature integration would require $O(N^2)$ steps.

Problem 2: Write a Fortran code to represent the initial state, introduced by Eq. (6), in the momentum space by applying the FFT algorithm to the grid-based representation generated in Problem 1. Visualize the result with Gnuplot. Represent the wave-packet amplitudes and phases in the range p=(-4,4) and compare

your output with the corresponding values obtained from the analytic Fourier transform obtained by using: $\int dx\ \exp(-a_2x^2+a_1x+a_0)=\sqrt{\pi/a_2}\ \exp(a_0+a_1^2/(4a_2))$.

Next, we consider the grid-based representation of operators (*e.g.*, $\hat{x}$, $\hat{p}$, $V(\hat{x})$, and $\hat{T}=\hat{p}^2/(2m)$) and learn how these operators act on states represented on grids in coordinate and momentum spaces.

Consider first applying the potential energy operator to the initial state, as follows,

$$V(\hat{x})\Psi_0(x)=V(x)\Psi_0(x)\equiv\tilde{\Psi}_0(x). \tag{12}$$

Since $\tilde{\Psi}_0(x)$ is just another function, Eq. (12) indicates that $V(\hat{x})$ can be represented on the same grid of coordinates as before (*i.e.*, equally spaced coordinates $x_j=x_{min}+(j-1)\Delta$, with finite resolution $\Delta=(x_{max}-x_{min})/(n-1)$). Since for each x_j, $\tilde{\Psi}_0(x_j)=V(x_j)\Psi(x_j)$, the operator $V(\hat{x})$ can be represented just as an array of numbers $V(x_j)$ associated with the grid-points x_j, and its operation on a state is represented on such a grid as a simple multiplication.

Problem 3: Write a Fortran code to compute the expectation values of the position $x(0)=\langle\Psi_0|\hat{x}|\Psi_0\rangle$ and the potential energy $V=\langle\Psi_0|V(\hat{x})|\Psi_0\rangle$, where $V(x)$ is defined according to Eq. (3) for the initial wave-packet, introduced by Eq. (6), with various possible values of x_0 and p_0, with $\alpha=\omega m$, where $m=1$ and $\omega=1$.

Now consider applying the momentum operator, $\hat{p}=-i\nabla$, to the initial state $\Psi_0(x)$ as follows,

$$G(x)=\langle x|\hat{p}|\Psi_0\rangle=-i\nabla\Psi_0(x). \tag{13}$$

One simple way of implementing this operation, when $\Psi_0(x)$ is represented on a grid of equally spaced points $x_j=x_{min}+(j-1)\Delta$, is by computing finite-increment derivatives as follows:

$$G(x_j)=-i\frac{\Psi_0(x_{j+1})-\Psi_0(x_{j-1})}{2\Delta}. \tag{14}$$

However, for a more general operator (*e.g.*, $\hat{T}=\hat{p}^2/(2m)$) this finite increment derivative procedure becomes complicated. In order to avoid computing finite-increment derivatives, one can implement an alternative procedure: represent the initial state in momentum-space (by Fourier transform of the initial state); apply the operator by simple multiplication in momentum space, then transform the resulting product back to the coordinate representation (by inverse-Fourier transform). This method can be derived by inserting the closure relation $\hat{1}=\int dp|p\rangle\langle p|$, in Eq. (13),

$$G(x)=\langle x|\hat{p}|\Psi_0\rangle=\int dp\langle x|\hat{p}|p\rangle\langle p|\Psi_0\rangle=(2\pi)^{-1/2}\int dpe^{ipx}p\langle p|\Psi_0\rangle, \tag{15}$$

since $\langle p|\Psi_0\rangle$ is defined, according to Eq. (10), as the Fourier transform of the initial state. Note that the second equality of Eq. (15) is obtained by introducing the substitution

$$\langle x|p\rangle=(2\pi)^{-1/2}e^{ix\hat{p}}. \tag{16}$$

While Eq. (15) illustrates the method for the specific operator $\hat{p}$, one immediately sees that any operator which is a function of $\hat{p}$ (*e.g.*, $\hat{T}=\hat{p}^2/(2m)$) can be analogously applied according to the Fourier transform procedure.

Problem 4: Write a Fortran code to compute the expectation values of the initial momentum $p(0)=\langle\Psi_0|\hat{p}|\Psi_0\rangle$ and the kinetic energy $T=\langle\Psi_0|\hat{p}^2/(2m)|\Psi_0\rangle$ by using the Fourier transform procedure, where Ψ_0 is the initial wave-packet introduced by Eq. (6), with $x_0=0$, $p_0=0$, and $\alpha=\omega m$, where $m=1$ and $\omega=1$. Compute the expectation value of the energy $E=\langle\Psi_0|\hat{H}|\Psi_0\rangle$, where $\hat{H}=\hat{p}^2/(2m)+V(\hat{x})$, with $V(x)$ defined according to Eq. (3) and compare your result with the zero-point energy $E_0=\omega/2$.

III SOFT Method

The Split-Operator Fourier Transform (SOFT) method is a numerical approach for solving the time-dependent Schrödinger equation by using grid-based representations of the time-evolving states and operators. It relies on the Fourier transform procedure, introduced in Sec. II, to apply operators that are functions of $\hat{p}$ by simple multiplication of array elements.

The essence of the method is to discretize the propagation time on a grid $t_k = (k-1)\tau$, with $k = 1, ..., n$ and time-resolution $\tau = t/(n-1)$, and obtain the wave-packet at the intermediate times t_k by recursively applying Eq. (2) as follows,

$$\Psi_{t_{k+1}}(x) = \int dx' \langle x|e^{-i\hat{H}\tau}|x'\rangle\langle x'|\Psi_{t_k}\rangle. \tag{17}$$

If τ is a sufficiently small time-increment (*i.e.*, n is large), the time-evolution operator can be approximated according to the Trotter expansion to second order accuracy,

$$e^{-i\hat{H}\tau} = e^{-iV(\hat{x})\tau/2}e^{-i\hat{p}^2\tau/(2m)}e^{-iV(\hat{x})\tau/2} + O(\tau^3), \tag{18}$$

which separates the propagator into a product of three operators, each of them depending either on $\hat{x}$, or $\hat{p}$.

Problem 5: Expand the exponential operators in both sides of Eq. (18) and show that the Trotter expansion is accurate to second order in powers of τ.

Substituting Eq. (18) into Eq. (17) and inserting the closure relation $\hat{\mathbf{1}} = \int dp|p\rangle\langle p|$ gives,

$$\Psi_{t_{k+1}}(x) = \int dp \int dx' e^{-iV(\hat{x})\tau/2}\langle x|p\rangle e^{-ip^2\tau/(2m)}\langle p|x'\rangle e^{-iV(x')\tau/2}\Psi_{t_k}(x'). \tag{19}$$

By substituting $\langle p|x'\rangle$ and $\langle x|p\rangle$ according to Eqs. (11) and (16), respectively, we obtain:

$$\Psi_{t_{k+1}}(x) = e^{-iV(\hat{x})\tau/2}\frac{1}{\sqrt{2\pi}}\int dp e^{ixp}e^{-ip^2\tau/(2m)}\frac{1}{\sqrt{2\pi}}\int dx' e^{-ipx'}e^{-iV(x')\tau/2}\Psi_{t_k}(x'). \tag{20}$$

According to Eq. (20), then, the computational task necessary to propagate $\Psi_t(x)$ for a time-increment τ involves the following steps:

1. Represent $\Psi_{t_k}(x')$ and $e^{-iV(x')\tau/2}$ as arrays of numbers $\Psi_{t_k}(x_j)$ and $e^{-iV(x_j)\tau/2}$ associated with a grid of equally spaced coordinates $x_j = x_{min} + (j-1)\Delta$, with finite resolution $\Delta = (x_{max} - x_{min})/(n-1)$.

2. Apply the potential energy part of the Trotter expansion $e^{-iV(x')\tau/2}$ to $\Psi_{t_k}(x')$ by simple multiplication of array elements:
$$\tilde{\Psi}_{t_k}(x_j) = e^{-iV(x_j)\tau/2}\Psi_{t_k}(x_j).$$

3. Fourier transform $\tilde{\Psi}_{t_k}(x_j)$ to obtain $\tilde{\Psi}_{t_k}(p_j)$, and represent the kinetic energy part of the Trotter expansion $e^{-ip^2\tau/(2m)}$ as an array of numbers $e^{-ip_j^2\tau/(2m)}$ associated with a grid of equally spaced momenta $p_j = j/(x_{max} - x_{min})$.

4. Apply the kinetic energy part of the Trotter expansion $e^{-ip^2\tau/(2m)}$ to the Fourier transform $\tilde{\Psi}_{t_k}(p)$ by simple multiplication of array elements:
$$\widetilde{\Psi}_{t_k}(p_j) = e^{-ip_j^2\tau/(2m)}\tilde{\Psi}_{t_k}(p_j).$$

5. Inverse Fourier transform $\widetilde{\Psi}_{t_k}(p_j)$ to obtain $\widetilde{\Psi}_{t_k}(x_j)$ on the grid of equally spaced coordinates x_j.

6. Apply the potential energy part of the Trotter expansion $e^{-iV(x')\tau/2}$ to $\widetilde{\Psi}_{t_k}(x')$ by simple multiplication of array elements,

$$\Psi_{t_{k+1}}(x_j) = e^{-iV(x_j)\tau/2}\widetilde{\Psi}_{t_k}(x_j).$$

Problem 6: Write a Fortran code that propagates the initial state $\Psi_0(x)$ for a single time increment ($\tau = 0.1$ a.u.). Use $x_0 = -2.5$, $p_0 = 0$, and $\alpha = \omega m$, where $m = 1$ and $\omega = 1$. Implement the SOFT method for the Hamiltonian $\hat{H} = \hat{p}^2/(2m) + V(\hat{x})$, where $V(x)$ is defined according to Eq. (3). Compare the resulting propagated state with the analytic solution obtained by substituting Eq. (5) into Eq. (2).

Problem 7: Loop the Fortran code developed in Problem 5 with $x_0 = -2.5$ and $p_0 = 0$ for 100 steps with $\tau = 0.1$ a.u. For each step compute the expectation values of coordinates $x(t)$ and momenta $p(t)$ as done in Problems 3 and 4, respectively. Compare your calculations with the analytic solutions obtained by substituting Eq. (5) into Eq. (2). Verify that these correspond to the classical trajectories $x(t) = \bar{x} + (x_0 - \bar{x})\text{cos}(\omega t)$ and $p(t) = p_0 - (x_0 - \bar{x})\omega m\ \text{sin}(\omega t)$, which can be computed according to the Velocity-Verlet algorithm:

$$\begin{aligned} p_{j+1} &= p_j + (F(x_j) + F(x_{j+1}))\tau/2 \\ x_{j+1} &= x_j + p_j\tau/m + F(x_j)\tau^2/(2m). \end{aligned} \tag{21}$$

Problem 8: Change the potential to that of a Morse oscillator $V(\hat{x}) = De(1 - \text{exp}(-a(\hat{x} - x_e)))^2$, with $x_e = 0$, $De = 8$, and $a = \sqrt{k/(2D_e)}$, where $k = m\omega^2$. Recompute the wave-packet propagation with $x_0 = -0.5$ and $p_0 = 0$ for 100 steps with $\tau = 0.1$ a.u., and compare the expectation values $x(t)$ and $p(t)$ with the corresponding classical trajectories obtained by recursively applying the Velocity-Verlet algorithm.

Problem 9: Simulate the propagation of a wave-packet with $x_0 = -5.5$ and initial momentum $p_0 = 2$ colliding with a barrier potential $V(x) = 3$, if abs$(x) < 0.5$, and $V(x) = 0$, otherwise. Hint: In order to avoid artificial recurrences you might need to add an absorbing imaginary potential $V_a(x) = i(\text{abs}(x) - 10)^4$, if abs$(x) > 10$, and $V_a(x) = 0$, otherwise.

IV SOFT Propagation on Multiple Surfaces

The goal of this section is to generalize the implementation of the SOFT method to the description of quantum dynamics on multiple coupled potential energy surfaces.

To keep the presentation as simple as possible, we consider a molecule with two-coupled electronic states described by the Hamiltonian,

$$\hat{H} = \hat{p}^2/(2m) + \hat{V}, \tag{22}$$

where $\hat{V} = \hat{V}_0 + \hat{V}_c$, with $\hat{V}_0 = V_1(\hat{\mathbf{x}})|1\rangle\langle 1| + V_2(\hat{\mathbf{x}})|2\rangle\langle 2|$ and $\hat{V}_c = V_c(\hat{\mathbf{x}})|1\rangle\langle 2| + V_c(\hat{\mathbf{x}})|2\rangle\langle 1|$.

The computational task ahead is to implement the SOFT method to compute the time-dependent wave-packet

$$|\Psi(\mathbf{x};t)\rangle = \varphi_1(\mathbf{x};t)|1\rangle + \varphi_2(\mathbf{x};t)|2\rangle, \tag{23}$$

given the initial conditions $\varphi_1(\mathbf{x};0)$ and $\varphi_2(\mathbf{x};0)$, where $\varphi_1(\mathbf{x};t)$ and $\varphi_2(\mathbf{x};t)$ are the time-dependent nuclear wave-packet components associated with the electronic states $|1\rangle$ and $|2\rangle$, respectively. Note that here the main challenges are that $\hat{V}_0$ and $\hat{V}_c$ do not commute, $|\Psi(\mathbf{x};t)\rangle$ involves two wave-packet components and $\hat{H}$ is a 2×2 matrix in the basis of $|1\rangle$ and $|2\rangle$.

A simple approach for propagating $\varphi_1(\mathbf{x};t)$ and $\varphi_2(\mathbf{x};t)$ involves the embedded form of the Trotter expansion,

$$e^{-i\hat{H}2\tau} \approx e^{-i\frac{\hat{\mathbf{p}}^2}{2m}\tau} e^{-iV(\hat{\mathbf{x}})2\tau} e^{-i\frac{\hat{\mathbf{p}}^2}{2m}\tau} \approx e^{-i\frac{\hat{\mathbf{p}}^2}{2m}\tau} e^{-iV_0(\hat{\mathbf{x}})\tau} e^{-iV_c(\hat{\mathbf{x}})2\tau} e^{-iV_0(\hat{\mathbf{x}})\tau} e^{-i\frac{\hat{\mathbf{p}}^2}{2m}\tau}, \tag{24}$$

which can be implemented in the basis of $|1\rangle$ and $|2\rangle$ according to the following steps:

- Step [I]. Apply the kinetic energy part of the Trotter expansion to both wave-packet components $\varphi_1(\mathbf{x};t)$ and $\varphi_2(\mathbf{x};t)$ for time τ, as follows,

$$\begin{pmatrix} \varphi_1'(\mathbf{x};t+\tau) \\ \varphi_2'(\mathbf{x};t+\tau) \end{pmatrix} = \begin{pmatrix} e^{-i\frac{\hat{\mathbf{p}}^2}{2m}\tau} & 0 \\ 0 & e^{-i\frac{\hat{\mathbf{p}}^2}{2m}\tau} \end{pmatrix} \begin{pmatrix} \varphi_1(\mathbf{x};t) \\ \varphi_2(\mathbf{x};t) \end{pmatrix}. \tag{25}$$

- Step [II]. Mix the two wave-packet components $\varphi_1'(\mathbf{x};t+\tau)$ and $\varphi_2'(\mathbf{x};t+\tau)$,

$$\begin{pmatrix} \varphi_1''(\mathbf{x};t+\tau) \\ \varphi_2''(\mathbf{x};t+\tau) \end{pmatrix} = \mathbf{M} \begin{pmatrix} \varphi_1'(\mathbf{x};t+\tau) \\ \varphi_2'(\mathbf{x};t+\tau) \end{pmatrix}, \tag{26}$$

  with

$$\mathbf{M} \equiv \mathbf{L}^{-1} \begin{pmatrix} e^{-iE_1(x)\tau} & 0 \\ 0 & e^{-iE_2(x)\tau} \end{pmatrix} \mathbf{L}, \tag{27}$$

  where $E_1(x)$ and $E_2(x)$ are the eigenvalues of the potential energy matrix $V = V_0 + V_c$ and $\mathbf{L}$ the matrix of column eigenvectors in the basis of diabatic states $|1\rangle$ and $|2\rangle$. Eigenvalues and eigenvectors of a symmetric matrix can be obtained by using the subroutines TRED2, TQLI and EIGSRT, as described in Numerical Recipes (Chapter 11).[9]

  While this is a general procedure, the specific case of interest involves a 2×2 Hermitian matrix V, for which the matrix $\mathbf{M}$ can be found analytically,

$$\mathbf{M} \equiv \begin{pmatrix} e^{-i\hat{V}_1(\hat{\mathbf{x}})2\tau}\cos(2V_c(\hat{\mathbf{x}})\tau) & -i\,\sin(2V_c(\hat{\mathbf{x}})\tau)\; e^{-i(\hat{V}_1(\hat{\mathbf{x}})+\hat{V}_2(\hat{\mathbf{x}}))\tau} \\ -i\,\sin(2V_c(\hat{\mathbf{x}})\tau)\; e^{-i(\hat{V}_1(\hat{\mathbf{x}})+\hat{V}_2(\hat{\mathbf{x}}))\tau} & \cos(2V_c(\hat{\mathbf{x}})\tau)\; e^{-i\hat{V}_2(\hat{\mathbf{x}})2\tau} \end{pmatrix}. \tag{28}$$

- Step [III]. Propagate $\varphi_1''(\mathbf{x};t+\tau)$ and $\varphi_2''(\mathbf{x};t+\tau)$ for time τ, according to the free-particle propagator, by applying the kinetic energy part of the Trotter expansion:

$$\begin{pmatrix} \varphi_1(\mathbf{x};t+2\tau) \\ \varphi_2(\mathbf{x};t+2\tau) \end{pmatrix} = \begin{pmatrix} e^{-i\frac{\hat{\mathbf{p}}^2}{2m}\tau} & 0 \\ 0 & e^{-i\frac{\hat{\mathbf{p}}^2}{2m}\tau} \end{pmatrix} \begin{pmatrix} \varphi_1''(\mathbf{x};t+\tau) \\ \varphi_2''(\mathbf{x};t+\tau) \end{pmatrix}. \tag{29}$$

In practice, however, step [III] is combined with step [I] of the next propagation time-slice for all but the last propagation time-increment.

Problem 10: (a) Derive Eq. (28) by considering that,

$$e^{-i\mathbf{V}_c 2\tau} = \mathbf{D}^\dagger \begin{pmatrix} e^{iV_c(\mathbf{x})2\tau} & 0 \\ 0 & e^{-iV_c(\mathbf{x})2\tau} \end{pmatrix} \mathbf{D}, \tag{30}$$

with

$$\mathbf{D} = \mathbf{D}^\dagger \equiv \begin{pmatrix} -1/\sqrt{2} & 1/\sqrt{2} \\ 1/\sqrt{2} & 1/\sqrt{2} \end{pmatrix}, \tag{31}$$

since

$$e^{-i\mathbf{V}_c 2\tau} = \mathbf{1} + (-i\mathbf{V}_c 2\tau) + \frac{1}{2!}(-i\mathbf{V}_c 2\tau)^2 + ..., \tag{32}$$

and

$$\mathbf{V}_c \equiv \begin{pmatrix} 0 & V_c(\mathbf{x}) \\ V_c(\mathbf{x}) & 0 \end{pmatrix} = \mathbf{D}^\dagger \begin{pmatrix} -V_c(\mathbf{x}) & 0 \\ 0 & V_c(\mathbf{x}) \end{pmatrix} \mathbf{D}, \tag{33}$$

with $\mathbf{D}\mathbf{D}^\dagger = 1$.

Problem 11: Derive Eq. (27) by writing the matrix V in the basis of adiabatic eigenstates

$$\begin{aligned} \phi_1(x) &= L_{11}(x)|1\rangle + L_{21}(x)|2\rangle, \\ \phi_2(x) &= L_{12}(x)|1\rangle + L_{22}(x)|2\rangle, \end{aligned} \tag{34}$$

with eigenvalues $E_1(x)$ and $E_2(x)$, respectively. Then, using the expansion

$$e^{-i\mathbf{V}2\tau} = \mathbf{1} + (-i\mathbf{V}2\tau) + \frac{1}{2!}(-i\mathbf{V}2\tau)^2 + ..., \tag{35}$$

show that in the adiabatic representation

$$e^{-i\mathbf{V}2\tau} = \begin{pmatrix} e^{-iE_1(x)2\tau} & 0 \\ 0 & e^{-iE_2(x)2\tau} \end{pmatrix}. \tag{36}$$

Finally, show that the diagonal matrix introduced by Eq. (36) can be rotated to the representation of diabatic states $|1\rangle$, $|2\rangle$ according to the similarity transformation

$$\mathbf{L}^{-1} \begin{pmatrix} e^{-iE_1(x)\tau} & 0 \\ 0 & e^{-iE_2(x)\tau} \end{pmatrix} \mathbf{L}. \tag{37}$$

Problem 12: (a) Write a Fortran code to implement the SOFT approach described in this section, where step [II] is numerically computed according to Eq. (27). Propagate $|\Psi(\mathbf{x};t)\rangle = \varphi_1(\mathbf{x};t)|1\rangle + \varphi_2(\mathbf{x};t)|2\rangle$, where $\varphi_1(\mathbf{x};0) = \varphi_1(\mathbf{x};0) = \Psi_0(x)$ and $\Psi_0(x)$ as defined in Eq. (6). Use $x_0 = -2.2$, $p_0 = 0$, $m = 1$, $\omega = 1$ and two coupled potential energy surfaces described by the potential energy matrix

$$V = \begin{pmatrix} V_1(x) & \delta \\ \delta & V_2(x) \end{pmatrix}, \tag{38}$$

where $\delta = 0.3$, $V_1(x) = m\omega^2(x - \bar{x})^2/2$ and $V_2(x) = -x^2/2 + x^4/22$; (b) Propagate $\Psi(\mathbf{x};t)$ according to the potential energy matrix introduced by Eq. (38), with $\delta = 0$ and compare your results with those obtained in item (a)

V Matching Pursuit Representation

The goal of this section is to generalize the grid-based representation of states, introduced in Sec. II, to representations generated according to the matching-pursuit algorithm as implemented for overcomplete basis sets of nonorthogonal basis functions.

The main advantage of overcomplete basis sets is that they provide non-unique representations, since there are multiple ways of expanding a target state as a linear combination of nonorthogonal basis functions (*i.e*, basis functions that can be expanded as linear combinations of the other basis functions in the

set). Therefore, one can define expansions that exploit the benefit of non-uniqueness in order to simultaneously achieve *sparsity* (*i.e.*, representations with the fewest possible significant terms), *superresolution* (*i.e.*, a resolution that is higher than that possible with traditional nonadaptive methods) and *speed* (i.e., representations obtainable in $O(n)$ or $O(n\log(n)$ steps, where n is the number of basis functions in the basis set.

The matching pursuit method implements a greedy algorithm for representing a target state (wavefunction) by successive orthogonal projections onto elements of an overcomplete basis set as follows: The first step requires selecting the basis element $\mid 1\rangle$ that has maximum overlap with the target state $\mid \Psi_t\rangle$ (*i.e.*, the element that is resonant with the most prominent structure in $\mid \Psi_t\rangle$). The projection of such element is defined as follows:

$$|\Psi_t\rangle = c_1|1\rangle + |\varepsilon_1\rangle, \tag{39}$$

where $c_1 \equiv \langle 1|\Psi_t\rangle$. Note that by virtue of the definition of c_1 the residual vector $|\varepsilon_1\rangle$ is orthogonal to $|1\rangle$. Therefore, $\|\Psi_t\| < \|\varepsilon_1\|$. The next step involves the sub-decomposition of the residual vector $|\varepsilon_1\rangle$ by projecting it along the direction of its best match $|2\rangle$ as follows:

$$|\varepsilon_1\rangle = c_2|2\rangle + |\varepsilon_2\rangle, \tag{40}$$

where $c_2 \equiv \langle 2|\varepsilon_1\rangle$. Note that, since $|\varepsilon_2\rangle$ is orthogonal to $|2\rangle$, the norm of $|\varepsilon_2\rangle$ is smaller than the norm of $|\varepsilon_1\rangle$. This procedure is repeated each time on the resulting residue.

After n successive orthogonal projections, the norm of the residual vector $|\varepsilon_n\rangle$ is smaller than a desired precision ϵ. Therefore, the algorithm maintains norm conservation within a desired precision,

$$\| \varepsilon_n \| = \sqrt{1 - \sum_{j=1}^{n} |c_j|^2} < \epsilon, \tag{41}$$

just as in a linear orthogonal decomposition. The resulting expansion is

$$\langle \mathbf{x}|\Psi_t\rangle \approx \sum_{j=1}^{n} c_j \langle \mathbf{x}|j\rangle, \tag{42}$$

where the coefficients c_j are recursively defined as follows:

$$c_j = \langle j|\Psi_t\rangle - \sum_{k=1}^{j-1} c_k \langle j|k\rangle. \tag{43}$$

Matching pursuit coherent-state expansions can be obtained by successively selecting the basis functions according to a gradient-based optimization technique.[10] A parallel implementation under the Message Passing Interface (MPI) environment[11] can speed up the search for a satisfactory local minimum. Starting from an initial trial coherent state $|\chi_j\rangle$, we can optimize the parameters $x_j(k)$, $p_j(k)$ and $\gamma_j(k)$ so that they locally maximize the overlap with the target state. Initial guess parameters $\gamma_j(k)$, $x_j(k)$ and $p_j(k)$ can be chosen as defined by the basis elements of the previous wave-packet representation (or initial state).

Problem 13: Write a Fortran code to represent the target state $\tilde{\Psi}_0(\mathbf{x}) \equiv e^{-i\hat{p}^2/(2m)\tau/2} e^{-iV(x)\tau} e^{-i\hat{p}^2/(2m)\tau/2} \Psi_0(x)$, where $\tau = 0.1$ a.u. and $V(x)$ is defined as in Problem 6, as a matching pursuit expansion based on coherent-states $|x_j, p_j, \gamma_j\rangle$ parametrized as follows:

$$\langle x|x_j, p_j, \gamma_j\rangle = \left(\frac{\gamma_j}{\pi}\right)^{1/4} e^{-\frac{\gamma_j}{2}(x-x_j)^2 + ip_j(x-x_0)}. \tag{44}$$

VI MP/SOFT Method for Adiabatic Propagation

The goal of this section is to introduce the implementation of the SOFT method for adiabatic quantum propagation, described in Sec. III, in terms of dynamically adaptive coherent-state representations generated according to the matching-pursuit algorithm introduced in Sec. V.

In order to implement the Trotter expansion,

$$\Psi_{t+\tau}(\mathbf{x}) = e^{-i[\frac{\hat{\mathbf{p}}^2}{2m}+V(\hat{\mathbf{x}})]\tau}\Psi_t(\mathbf{x}) \approx e^{-iV(\hat{\mathbf{x}})\tau/2}e^{-i\hat{\mathbf{p}}^2/(2m)\tau}e^{-iV(\hat{\mathbf{x}})\tau/2}\Psi_t(\mathbf{x}), \tag{45}$$

by using representations based on matching-pursuit coherent-state expansions, one can proceed according to the following steps:

- Step 1. Decompose the target function $\tilde{\Psi}_t(\mathbf{x}) \equiv e^{-iV(\hat{\mathbf{x}})\tau/2}\Psi_t(\mathbf{x})$ into matching pursuit coherent state expansions,

$$\tilde{\Psi}_t(\mathbf{x}) \approx \sum_{j=1}^{n} c_j \langle \mathbf{x}|\chi_j\rangle. \tag{46}$$

  Here, $\langle \mathbf{x}|\chi_j\rangle$ are N-dimensional coherent states,

$$\langle \mathbf{x}|\chi_j\rangle \equiv \prod_{k=1}^{N} A_j(k)\exp\left(-\frac{\gamma_j(k)}{2}(x(k)-x_j(k))^2 + ip_j(k)(x(k)-x_j(k))\right), \tag{47}$$

  where $A_j(k)$ are normalization factors and $\gamma_j(k)$, $x_j(k)$ and $p_j(k)$ are complex-valued parameters selected according to the matching pursuit algorithm. The expansion coefficients c_j, introduced by Eq. (46), are defined before: $c_1 \equiv \langle \chi_1|\Psi_t\rangle$, and $c_j \equiv \langle \chi_j|\Psi_t\rangle - \sum_{k=1}^{j-1} c_k\langle \chi_j|\chi_k\rangle$, for $j = 2$–N.

- Step 2. Apply the kinetic energy part of the Trotter expansion to $\tilde{\Psi}_t(\mathbf{x})$ by Fourier transforming the coherent state expansion of $\tilde{\Psi}_t(\mathbf{x})$ to the momentum representation, multiplying it by $\exp[-i(\mathbf{p}^2/2m)\tau]$ and finally computing the inverse Fourier transform of the product to obtain:

$$\widetilde{\Psi}_t(\mathbf{x}) = \sum_{j=1}^{n} c_j \langle \mathbf{x}|\tilde{\chi}_j\rangle, \tag{48}$$

  where

$$\langle \mathbf{x}|\tilde{\chi}_j\rangle \equiv \prod_{k=1}^{N} A_j(k)\sqrt{\frac{m}{m+i\tau\gamma_j(k)}}\exp\left(\frac{\left(\frac{p_j(k)}{\gamma_j(k)} - i[x_j(k)-x(k)]\right)^2}{\frac{2}{\gamma_j(k)}+\frac{2i\tau}{m}} - \frac{p_j(k)}{2\gamma_j(k)}\right). \tag{49}$$

  The resulting time-evolved wave-function is thus

$$\Psi_{t+\tau}(\mathbf{x}) = \sum_{j=1}^{n} c_j e^{-iV(\mathbf{x})\tau/2}\langle \mathbf{x}|\tilde{\chi}_j\rangle, \tag{50}$$

  which can be re-expanded in coherent states as in step [1].

Note that the underlying computational task necessary for MP/SOFT quantum propagation is completely reduced to generating the coherent-state expansions defined by Eq. (46), since all of the other steps can be implemented analytically.

Problem 14: Note that the Fortran code developed in Problem 13 already implements the MP/SOFT method described in this section, as applied to the Harmonic potential of Problem 5. Now, loop the code for 100 steps and make the comparison between numerical and analytical results for the whole propagation time. Use ($\tau = 0.1$ a.u.) with $x_0 = -2.5$, $p_0 = 0$, and $\alpha = \omega m$, where $m = 1$ and $\omega = 1$.

VII MP/SOFT Simulations of Nonadiabatic Dynamics in Pyrazine

MP/SOFT simulations of nonadiabatic dynamics can be efficiently performed according to the SOFT method outlined in Sec. IV, in conjunction with the matching-pursuit representation method introduced in Sec. V. The goal of this section is to illustrate the resulting approach as applied to the description of the S_1/S_2 interconversion of pyrazine after $S_0 \rightarrow S_2$ photoexcitation. The photophysics of pyrazine provides a standard platform for study ultrafast internal conversion responsible for a broad band photoabsorption spectrum with a rather diffuse superimposed structure. The underlying excited state nonadiabatic dynamics, following $S_0 \rightarrow S_1(\pi,\pi^*)$, $S_2(n,\pi^*)$ photoexcitation, is also ideally suited to benchmark the capabilities of new theoretical methods since it has been extensively investigated both experimentally[12,13] and theoretically.[14–20] *Ab initio* calculations have characterized the existence of a conical intersection between the S_1 and S_2 states, leading to ultrafast intramolecular energy transfer.[14] The experimental S_2 photoabsorption spectrum has been reproduced by using a 4-mode model Hamiltonian, after convoluting the resulting spectrum with an experimental resolution function,[21] or explicitly including the effect of the remaining vibrational modes as a weakly coupled harmonic bath.[15] These two models have allowed for direct comparisons between benchmark calculations and state-of-the-art semiclassical and quantum mechanical methods, including the multiconfigurational time dependent Hartree (MCTDH) approach,[15] the Herman Kluk semiclassical initial value representation (SC IVR) method,[17] the multiple spawning quantum approach,[18] the time dependent Gauss-Hermite discrete value representation (TDGH-DVR) method,[19] and the coupled coherent states (CCS) technique.[20] Here, the capabilities of the generalized MP/SOFT approach are evaluated as applied to the description of the photoabsorption spectroscopy of pyrazine.

The problem concerns the propagation of the wave-packet components $\varphi_1(\mathbf{x};t)$ and $\varphi_2(\mathbf{x};t)$, introduced by Eq. (23), as the molecule undergoes excited state interconversion dynamics at the conical intersection of the S_1 and S_2 coupled potential energy surfaces. Therefore, it can be assumed that the initial state is defined according to Eq. (23) in terms of the two ground vibrational state wave-packet components,

$$\begin{aligned} \varphi_1(\mathbf{x};0) &= 0, \\ \varphi_2(\mathbf{x};0) &= \prod_{j=1}^{N} \left(\frac{1}{\pi}\right)^{1/4} e^{-x(j)^2/2}, \end{aligned} \tag{51}$$

associated with the S_1 and S_2 states, respectively. Here, N is the dimensionality of the system, as defined by the number of vibrational modes explicitly considered in the model (*i.e.*, $N = 4$ in the reduced model system, and $N = 24$ in the full-dimensional model).

The S_2 photoabsorption spectrum $I(\omega)$ can be computed as the Fourier transform of the survival amplitude $C(t)$,

$$I(\omega) \propto \omega \int_{\infty}^{\infty} dt C(t) e^{i(\omega+\epsilon_0)t}, \tag{52}$$

where ϵ_0 denotes the energy of the ground vibrational state of pyrazine, and $\omega = 2\pi c/\lambda$. The time-dependent survival amplitude,

$$C(t) = \langle \Psi(0) | e^{-i\hat{H}t} | \Psi(0) \rangle = \int d\mathbf{x} \Psi^{\star}(\mathbf{x}; -t/2) \Psi(\mathbf{x}; t/2), \tag{53}$$

is obtained by overlapping the time-evolved states $\Psi(\mathbf{x};t/2) = e^{-i\hat{H}t/2}\Psi(\mathbf{x};0)$ and $\Psi(\mathbf{x};-t/2) = e^{i\hat{H}t/2}\Psi(\mathbf{x};0)$, after propagating the initial state $\Psi(\mathbf{x};0)$ forward and backward in time on the nonadiabatically coupled excited electronic states. Here, $\Psi(\mathbf{x};0)$ is the initial ground state wavefunction, multiplied by the transition dipole moment which is assumed to be constant as a function of nuclear coordinates (Condon approximation).

The Hamiltonian $\hat{H} = \hat{H}_0 + \hat{V}_c$ of pyrazine is defined as follows:

$$\hat{H}_0 = \sum_j -\frac{1}{2m_j}\frac{\partial^2}{\partial Q_j^2}\left(|1\rangle\langle 1| + |2\rangle\langle 2|\right) + \sum_j \frac{1}{2} m_j \omega_j^2 Q_j^2 \left(|1\rangle\langle 1| + |2\rangle\langle 2|\right) + \Delta\left(|2\rangle\langle 2| - |1\rangle\langle 1|\right) + \sum_{i\in G_1}\left(a_i|1\rangle\langle 1| + b_i|2\rangle\langle 2|\right) Q_i + \sum_{(i,j)\in G_2}\left(a_{i,j}|1\rangle\langle 1| + b_{i,j}|2\rangle\langle 2|\right) Q_i Q_j, \tag{54}$$

and

$$\hat{V}_c = \sum_{i\in G_3} c_i \left(|1\rangle\langle 2| + |2\rangle\langle 1|\right) Q_i + \sum_{(i,j)\in G_4} c_{i,j}\left(|1\rangle\langle 2| + |2\rangle\langle 1|\right) Q_i Q_j. \tag{55}$$

The parameters introduced by these equations are readily available in Ref. [15] and have been obtained at the complete-active-space self-consistent-field (CASSCF) *ab initio* level,[21] including a total of 102 coupling constants a_i, b_i, c_i, $a_{i,j}$, $b_{i,j}$ and $c_{i,j}$, explicitly describing the 24 vibrational modes of pyrazine. In addition, to facilitate the comparison with experimental data, the 24-dimensional potential energy surfaces should be shifted in energy by 4.06 eV. A more recent set of parameters has been kindly supplied by Meyer and co-workers and is available upon request.

The first and second terms, introduced by Eq. (54), define the harmonic expansion of the diabatic surfaces, where ω_j are the experimental ground-state vibrational frequencies, and $m_j = \omega_j^{-1}$. Further, $Q_j = (x_j - x_j^{eq})/(m_j\omega_j)^{-1/2}$ are the dimensionless normal-mode coordinates. The third term in Eq. (54) introduces the couplings between the S_1 and S_2 potential energy surfaces at the ground-state equilibrium configuration ($\mathbf{Q} = 0$). The fourth and fifth terms in Eq. (54) include the linear and quadratic contributions to the diabatic-state expansions, where G_1 and G_2 indicate the set of modes having A_g and B_{2g} symmetry, respectively. The nonadiabatic couplings are described to second order accuracy, as given by Eq. (55), where G_3 represents the modes with symmetry B_{1g} that linearly couple the S_1 and S_2 states, and G_4 is the set of all pairs of modes the product of which has B_{1g} symmetry, including the combinations $A_g \times B_{1g}$, $B_{2g} \times B_{3g}$, $A_u \times B_{1u}$, and $B_{2u} \times B_{3u}$.

A reduced 4-mode model can be constructed by following earlier work,[15] including only the vibronic coupling mode ν_{10a} and the three totally symmetric modes with the strongest linear coupling parameters, ν_{6a}, ν_1 and ν_{9a}. In addition, to facilitate the comparison with experimental data, the 4-dimensional potential energy surfaces should be shifted in energy by 3.94 eV.

Problem 15: (a) Assuming that the initial state of pyrazine is defined according to Eq. (51), obtain the analytic expressions of $\varphi_1'(\mathbf{x};\tau)$ and $\varphi_2'(\mathbf{x};\tau)$, as defined in Eq. (25); (b) Modify the Fortran code developed in Problem 13 in order to implement Eq. (26), defining the coupling matrix $\mathbf{M}$ in accord with Eq. (28) and the model Hamiltonian introduced by the Eqs. (54) and (55). Hint: Express the sine and cosine functions, introduced by Eq. (28), in terms of exponentials and compute the Gaussian integrals analytically by using $\int dx\, \exp(-a_2x^2 + a_1x + a_0) = \sqrt{\pi/a_2}\, \exp(a_0 + a_1^2/(4a_2))$. (c) Loop the code and propagate the wave-packet for the 4-dimensional and the full-dimensional models, storing the wave-packet at all intermediate times. (d) Compute the survival amplitude as defined in Eq. (53) and the photoabsorption spectrum $I(\omega)$, as the Fourier transform of the survival amplitude $C(t)$, introduced by Eq. (52). Check your results as compared to earlier calculations.[15,17–20]

VIII MP/SOFT Computations of Thermal Correlation Functions

The goal of this section is to introduce a generalization of the MP/SOFT method for the description of thermal-equilibrium density matrices, finite-temperature time-dependent expectation values and time-correlation functions.

Consider the problem of computing thermal correlation functions,

$$C(t) = \langle A(0)B(t)\rangle = Z^{-1}\mathsf{Tr}[e^{-\beta\hat{H}_0}\hat{A}e^{i\hat{H}_1 t}\hat{B}e^{-i\hat{H}_1 t}], \tag{56}$$

where $\langle\cdots\rangle$ indicates the Boltzmann ensemble average at temperature $T = 1/(k_B\beta)$, with k_B the Boltzmann constant; $\hat{A}$ and $\hat{B}$ are quantum-mechanical operators associated with measurements of observables at time 0 and t, respectively; $Z = \mathsf{Tr}[e^{-\beta\hat{H}_0}]$ is the canonical partition function; and $\hat{H}_j = -\nabla^2_{\mathbf{x}}/(2m) + V_j(\hat{\mathbf{x}})$ is the Hamiltonian of the system of interest with N degrees of freedom interacting according to the potential $V_j(\hat{\mathbf{x}})$. An example is the correlation function $C(t)$ for a system evolving on the excited state potential energy surface $V_1(\hat{\mathbf{x}})$, as would result from a photoexcitation process after the initial preparation at thermal-equilibrium in the ground state potential energy surface $V_0(\hat{\mathbf{x}})$. To keep the notation as simple as possible, all expressions are written in mass-weighted coordinates and atomic units, so that all degrees of freedom have the same mass m and $\hbar = 1$.

Note that Eq. (56) provides an expression for computing not only time-dependent thermal correlation functions but also thermal-equilibrium ensemble averages $\langle A\rangle = Z^{-1}\mathsf{Tr}[e^{-\beta\hat{H}_0}\hat{A}]$, when $\hat{B} = 1$, and finite-temperature time-dependent ensemble averages,

$$\langle B(t)\rangle = Z^{-1}\mathsf{Tr}[e^{-\beta\hat{H}_0}e^{i\hat{H}_1 t}\hat{B}e^{-i\hat{H}_1 t}], \tag{57}$$

when $\hat{A} = 1$.

Thermal correlation functions $C(t)$ are obtained according to the following symmetrized form of Eq. (56):

$$C(t) = Z^{-1}\int d\mathbf{x}\int d\mathbf{x}'\int d\mathbf{x}''\langle\mathbf{x}|e^{-\frac{\beta}{2}\hat{H}_0}|\mathbf{x}'\rangle A(\mathbf{x}')\langle\mathbf{x}'|e^{i\hat{H}_1 t}\hat{B}e^{-i\hat{H}_1 t}|\mathbf{x}''\rangle\langle\mathbf{x}''|e^{-\frac{\beta}{2}\hat{H}_0}|\mathbf{x}\rangle. \tag{58}$$

The computational task necessary to obtain $C(t)$, according to Eq. (58), requires obtaining the matrix elements $A(\mathbf{x}')\langle\mathbf{x}'|e^{-\frac{\beta}{2}\hat{H}_0}|\mathbf{x}\rangle$ and $\langle\mathbf{x}''|e^{-\frac{\beta}{2}\hat{H}_0}|\mathbf{x}\rangle$ and the subsequent real-time propagation for time t, according to $\hat{H}_1$. The matrix elements are computed, as described below by imaginary-time integration of the Bloch equation according to $\hat{H}_0$. The extension of the MP/SOFT method, introduced in this section, involves the numerically exact treatment of both the real- and imaginary-time propagation steps as described below for the imaginary-time propagation. The real-time propagation is analogously performed by simply implementing the variable transformation $\beta \to -it$ from imaginary to real time.

The Boltzmann-operator matrix-elements are obtained by solving the Bloch equation,[22]

$$\{\frac{\partial}{\partial\beta} - \frac{1}{2m}\nabla^2_{\mathbf{x}} + V_0(\mathbf{x})\}\rho(\mathbf{x},\mathbf{x}';\beta) = 0, \tag{59}$$

for $\rho(\mathbf{x},\mathbf{x}';\beta) \equiv \langle\mathbf{x}|e^{-\beta\hat{H}_0}|\mathbf{x}'\rangle$ subject to the initial condition given by the high-temperature approximation,

$$\rho(\mathbf{x},\mathbf{x}';\epsilon) = \Big(\frac{m}{2\pi\epsilon}\Big)^{1/2} e^{-\frac{\epsilon}{2}[V_0(\mathbf{x})+V_0(\mathbf{x}')]}e^{-\frac{m}{2\epsilon}(\mathbf{x}-\mathbf{x}')^2}, \tag{60}$$

where ϵ defines a sufficiently high temperature $T = 1/(k_B\epsilon)$.

Equation (59) is formally integrated as follows,

$$\rho(\mathbf{x},\mathbf{x}';\beta) = \int d\mathbf{x}''\rho(\mathbf{x},\mathbf{x}'';\beta-\epsilon)\rho(\mathbf{x}'',\mathbf{x}';\epsilon), \tag{61}$$

where the propagator $\rho(\mathbf{x},\mathbf{x}'';\beta-\epsilon) \equiv \langle\mathbf{x}|e^{-(\beta-\epsilon)\hat{H}_0}|\mathbf{x}''\rangle$ is imaginary-time sliced by repeatedly inserting the resolution of identity,

$$\hat{\mathbf{1}} = \int d\mathbf{x}_j|\mathbf{x}_j\rangle\langle\mathbf{x}_j|, \tag{62}$$

yielding,

$$\langle \mathbf{x}|e^{-(\beta-\epsilon)\hat{H}_0}|\mathbf{x}''\rangle = \int d\mathbf{x}_{s-1}... \int d\mathbf{x}_1 \langle \mathbf{x}|e^{-i\hat{H}_0\tau}|\mathbf{x}_{s-1}\rangle ... \langle \mathbf{x}_1|e^{-i\hat{H}_0\tau}|\mathbf{x}''\rangle, \tag{63}$$

where $\tau \equiv -i(\beta-\epsilon)/s$ is a sufficiently thin imaginary-time slice.

Each finite-time propagator, introduced by Eq. (63), is approximated for sufficiently small imaginary-time slices τ by the Trotter expansion to second-order accuracy,

$$e^{-i\ \hat{H}_0\tau} \approx e^{-i\ V_0(\hat{\mathbf{x}})\tau/2} e^{-i\ \frac{\hat{\mathbf{p}}^2}{2m}\tau}\ e^{-i\ V_0(\hat{\mathbf{x}})\tau/2}. \tag{64}$$

The MP/SOFT propagation of the initial condition, introduced by Eq. (60), is performed according to the Trotter expansion introduced by Eq. (64) entailing the following steps:

- Step [1]: Decompose $\tilde{\rho}(\mathbf{x},\mathbf{x}';\epsilon) \equiv e^{-iV_0(\mathbf{x})\tau/2}\rho(\mathbf{x},\mathbf{x}';\epsilon)$ in a matching-pursuit coherent-state expansion:

$$\tilde{\rho}(\mathbf{x},\mathbf{x}';\epsilon) \approx \sum_{j=1}^{n} c_j \phi_j(\mathbf{x})[\phi'_j(\mathbf{x}')]^*, \tag{65}$$

  where $\phi_j(\mathbf{x})$ and $\phi'_j(\mathbf{x})$ are N-dimensional coherent-states defined as follows,

$$\phi_j(\mathbf{x}) \equiv \prod_{k=1}^{N} A_{\phi_j}(k) e^{-\gamma_{\phi_j}(k)\left(x(k)-x_{\phi_j}(k)\right)^2/2} e^{i\ p_{\phi_j}(k)\left(x(k)-x_{\phi_j}(k)\right)}, \tag{66}$$

  with complex-valued coordinates $x_{\phi_j}(k) \equiv r_{\phi_j}(k) + id_{\phi_j}(k)$, momenta $p_{\phi_j}(k) \equiv g_{\phi_j}(k) + if_{\phi_j}(k)$ and scaling parameters $\gamma_{\phi_j}(k) \equiv a_{\phi_j}(k) + ib_{\phi_j}(k)$. The normalization constants are

$$A_j(k) = \left(\frac{a_j(k)}{\pi}\right)^{1/4} \text{exp}[-\frac{1}{2}a_j(k)d_j(k)^2]\text{exp}[-d_j(k)g_j(k) - \frac{1}{2a_j(k)}\left(b_j(k)d_j(k)+f_j(k)\right)^2]. \tag{67}$$

  The expansion coefficients, introduced by Eq. (65), are defined as follows:

$$c_j \equiv \begin{cases} I_j, & \text{when} \quad j=1, \\ I_j - \sum_{k=1}^{j-1} c_k \langle \phi_j|\phi_k\rangle\langle \phi'_k|\phi'_j\rangle, & \text{for} \quad j = 2-n, \end{cases} \tag{68}$$

  where the overlap integral I_j is defined as follows,

$$I_j \equiv \int d\mathbf{x}' d\mathbf{x}\ \phi_j(\mathbf{x})\tilde{\rho}(\mathbf{x},\mathbf{x}';\epsilon)[\phi'_j(\mathbf{x}')]^*. \tag{69}$$

- Step [2]: Analytically Fourier transform the coherent-state expansion to the momentum representation, apply the kinetic energy part of the Trotter expansion and analytically inverse Fourier transform the resulting expression back to the coordinate representation to obtain the imaginary-time evolved Boltzmann-operator matrix elements:

$$\rho(\mathbf{x},\mathbf{x}';\epsilon+i\tau) = \sum_{j=1}^{n} c_j e^{-iV_0(\mathbf{x})\tau/2}\widetilde{\phi}_j(\mathbf{x})[\phi'_j(\mathbf{x}')]^*, \tag{70}$$

  where

$$\widetilde{\phi}_j(\mathbf{x}) \equiv \prod_{k=1}^{N} A_{\widetilde{\phi}_j}(k)\sqrt{\frac{m}{m+i\tau\gamma_{\widetilde{\phi}_j}(k)}}\text{exp}\left(\frac{\left(\frac{p_{\widetilde{\phi}_j}(k)}{\gamma_{\widetilde{\phi}_j}(k)} - i(x_{\widetilde{\phi}_j}(k)-x(k))\right)^2}{\left(\frac{2}{\gamma_{\widetilde{\phi}_j}(k)}+\frac{i2\tau}{m}\right)} - \frac{p_{\widetilde{\phi}_j}(k)^2}{2\gamma_{\widetilde{\phi}_j}(k)}\right). \tag{71}$$

Note that the MP/SOFT approach reduces the computational task necessary for the imaginary- or real-time propagation of the Boltzmann operator matrix elements $\rho(\mathbf{x},\mathbf{x}';\beta)$ to the problem of recursively generating the coherent-state expansions introduced by Eq. (65).

Coherent-state expansions are obtained as before by combining the matching pursuit algorithm and a gradient-based optimization method as follows:

- Step [1.1]. Evolve the complex-valued parameters, that define the initial trial coherent-states $\phi_j(\mathbf{x})$ and $\phi'_j(\mathbf{x})$, to locally maximize the overlap integral I_j, introduced in Eq. (69). Parameters $x_{\phi_1}(k), p_{\phi_1}(k), \gamma_{\phi_1}(k)$ and $x_{\phi'_1}(k), p_{\phi'_1}(k), \gamma_{\phi'_1}(k)$ of the corresponding local maximum define the first pair of coherent-states ϕ_1 and ϕ'_1 in the expansion introduced by Eq. (65) and the first expansion coefficient c_1, as follows: $\tilde{\rho}(\mathbf{x},\mathbf{x}';\epsilon) = c_1\phi_1(\mathbf{x})[\phi'_1(\mathbf{x}')]^* + \varepsilon_1(\mathbf{x},\mathbf{x}')$, where $c_1 \equiv I_1$, as defined according to Eq. (69). Note that due to the definition of c_1, the residue $\varepsilon_1(\mathbf{x},\mathbf{x}')$ does not overlap with the product state $\phi_1(\mathbf{x})[\phi'_1(\mathbf{x}')]^*$. Therefore, the norm of the remaining residue $\varepsilon_1(\mathbf{x},\mathbf{x}')$ is smaller than the norm of the initial target state $\tilde{\rho}(\mathbf{x},\mathbf{x}';\epsilon)$ —*i.e.*, $\| \varepsilon_1 \| < \| \tilde{\rho} \|$.

- Step [1.2]. Goto [1.1], replacing $\tilde{\rho}(\mathbf{x},\mathbf{x}';\epsilon)$ by $\varepsilon_1(\mathbf{x},\mathbf{x}')$ —*i.e.*, sub-decompose the residue by its projection along the direction of its locally optimum match as follows: $\varepsilon_1(\mathbf{x},\mathbf{x}') = c_2\phi_2(\mathbf{x})[\phi'_2(\mathbf{x}')]^* + \varepsilon_2(\mathbf{x},\mathbf{x}')$, where
$$c_2 \equiv \int d\mathbf{x}' d\mathbf{x}\ \phi_2(\mathbf{x})\varepsilon_1(\mathbf{x},\mathbf{x}')[\phi'_2(\mathbf{x}')]^*. \tag{72}$$
Note that $\| \varepsilon_2 \| < \| \varepsilon_1 \|$, since $\varepsilon_2(\mathbf{x},\mathbf{x}')$ is orthogonal to the product state $\phi_2(\mathbf{x})[\phi'_2(\mathbf{x}')]^*$.

Step [1.2] is repeated each time on the resulting residue. After n successive projections, the norm of the residue ε_n is smaller than a desired precision ϵ —*i.e.*, $\| \varepsilon_n \| = (1 - \sum_{j=1}^{n} |c_j|^2)^{1/2} < \epsilon$, and the resulting expansion is given by Eq. (65).

It is important to mention that the computational bottleneck of the MP/SOFT method involves the calculation of overlap matrix elements $\langle\phi_j|e^{-iV_j(\hat{\mathbf{x}})\tau/2}|\widetilde{\phi}_k\rangle$ and $\langle\phi_j|e^{-iV_j(\hat{\mathbf{x}})\tau/2}|\phi_k\rangle$, where $|\phi_k\rangle$ and $|\widetilde{\phi}_k\rangle$ are localized Gaussians introduced by Eqs. (66) and (71), respectively. The underlying computational task is however trivially parallelized according to a portable Single-Program-Multiple-Data streams code that runs under the Message-Passing-Interface (MPI) environment.

The overlap integrals are most efficiently computed in applications to reaction surface Hamiltonians where a large number of harmonic modes can be *arbitrarily* coupled to a few reaction (tunneling) coordinates (see, *e.g.*, Models I and II in Ref. [3] and the reaction surface Hamiltonians in Refs. [23–25]). For such systems, the Gaussian integrals over harmonic coordinates can be analytically computed and the remaining integrals over reaction coordinates are efficiently obtained according to numerical quadrature techniques. For more general Hamiltonians, the overlap matrix elements can be approximated by analytic Gaussian integrals when the choice of width parameters $\gamma_j(k)$ allows for a local expansion of $V_j(\hat{\mathbf{x}})$ to second order accuracy. Otherwise, the quadratic approximation is useful for numerically computing the corresponding full-dimensional integrals according to variance-reduction Monte Carlo techniques.

Problem 16: Evaluate the accuracy and efficiency of the MP/SOFT methodology in terms of explicit calculations of time-dependent position ensemble averages and position-position thermal correlation functions for the asymmetric quartic oscillator described by the following Hamiltonian:

$$\hat{H}_1 = \frac{\hat{p}^2}{2m} + V_1(x), \tag{73}$$

where

$$V_1(x) = \frac{1}{2}m\omega^2 x^2 - cx^3 + cx^4, \tag{74}$$

with $m = 1$ a.u., $\omega = \sqrt{2}$ a.u., and $c = 0.1$ a.u. The system is initially prepared at thermal equilibrium, with $\beta = 0.5$ a.u. on the displaced potential energy surface,

$$V_0(x) = \frac{1}{2} m\omega^2 (x-a)^2 - c(x-a)^3 + c(x-a)^4, \tag{75}$$

with $a = 1$ a.u. Check your results as compared to earlier calculations.[4,26–28]

The model system, introduced by Eqs. (73)—(75), is particularly interesting since the highly anharmonic potential leads to ultrafast dephasing within a few oscillation periods as well as later rephasing of wavepacket motion due to the effect of quantum coherences. The underlying dynamics can be described by rigorous quantum-mechanical approaches and has been investigated in terms of semiclassical approaches based on coherent-state representations.[4,26–28] Therefore, the model is ideally suited for a rigorous analysis of the accuracy and efficiency of the MP/SOFT method as compared to classical, semiclassical and benchmark quantum-mechanical calculations.

IX Acknowledgments

V.S.B. acknowledges supercomputer time from the National Energy Research Scientific Computing (NERSC)Center and financial support from Research Corporation, Research Innovation Award # RI0702, a Petroleum Research Fund Award from the American Chemical Society PRF # 37789-G6, a junior faculty award from the F. Warren Hellman Family, the National Science Foundation (NSF) Career Program Award CHE # 0345984, the NSF Nanoscale Exploratory Research (NER) Award ECS # 0404191, the Alfred P. Sloan Fellowship (2005-2006) from the Sloan Foundation, a Camille Dreyfus Teacher-Scholar Award for 2005, a Yale Junior Faculty Fellowship in the Natural Sciences (2005), and start-up package funds from the Provost's office at Yale University.

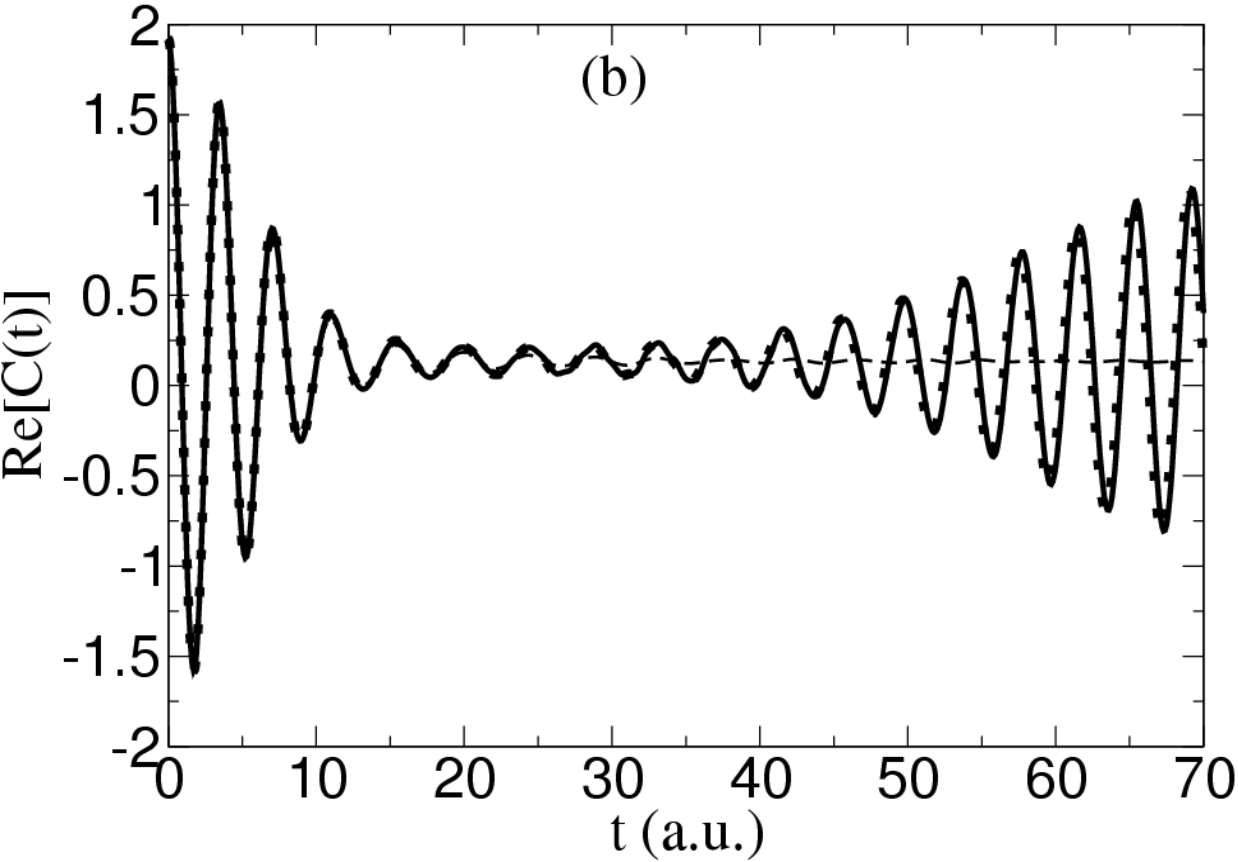
(b)
Re[C(t)]
t (a.u.)
2
1.5
1
0.5
0
-0.5
-1
-1.5
-2
0
10
20
30
40
50
60
70

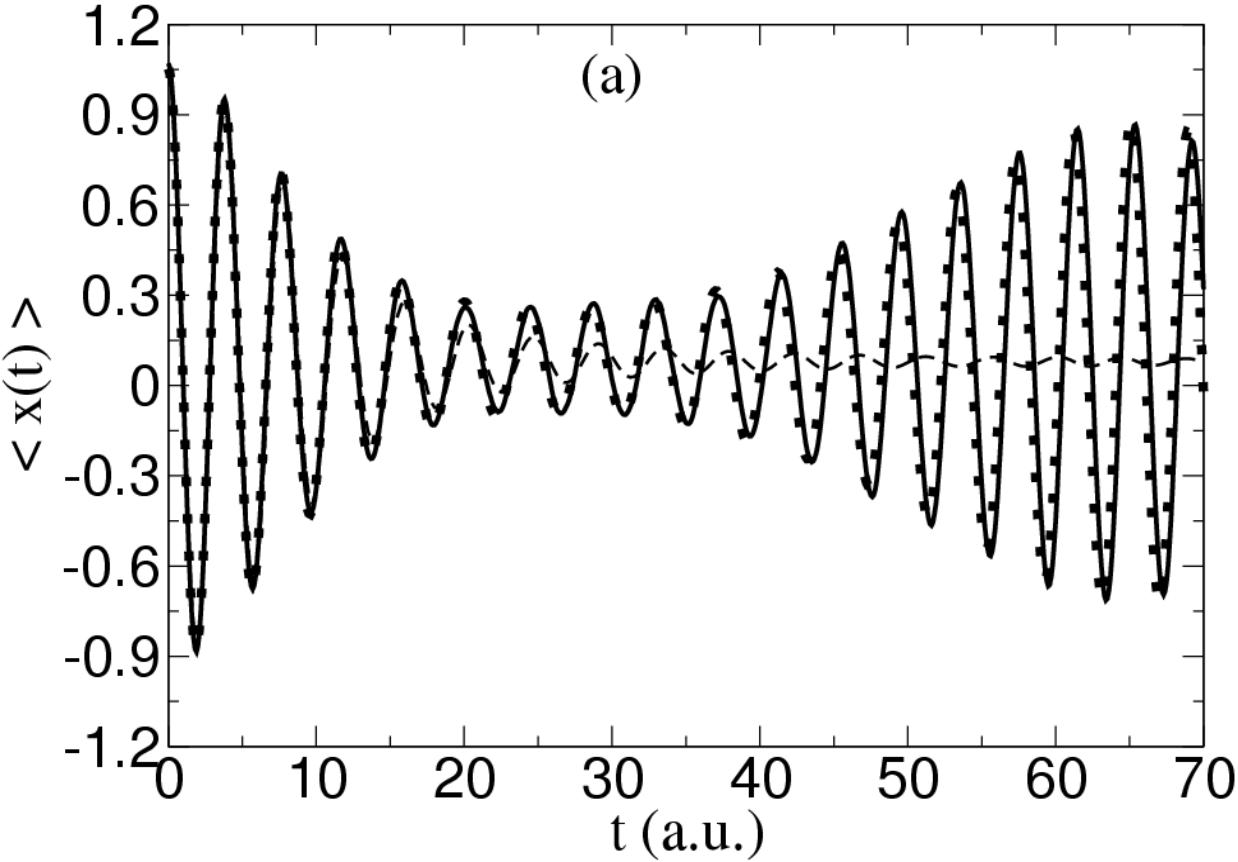
(a)
1.2
0.9
0.6
0.3
0
-0.3
-0.6
-0.9
-1.2
< x(t) >
0
10
20
30
40
50
60
70
t (a.u.)

References

[1] Y. Wu and V. S. Batista. *J. Chem. Phys.*, 118:6720, 2003.

[2] Y. Wu and V. S. Batista. *J. Chem. Phys.*, 119:7606, 2003.

[3] Y. Wu and V. S. Batista. *J. Chem. Phys.*, 121:1676, 2004.

[4] X. Chen, Y. Wu, and V. S. Batista. *J. Chem. Phys.*, 122:64102, 2005.

[5] Y. Wu, M. F. Herman, and V. S. Batista. *J. Chem. Phys.*, 122:114114, 2005.

[6] Y. Wu and V. S. Batista. *J. Chem. Phys.*, 124:224305, 2006.

[7] X. Chen and V. S. Batista. *J. Chem. Phys.*, 2006. submitted.

[8] W. H. Press, B. P. Flannery, S. A. Teukolsky, and W. T. Vetterling. In *Numerical Recipes*, chapter 12. Cambridge University Press, Cambridge, 1986. (http://www.library.cornell.edu/nr/bookfpdf/f12-2.pdf).

[9] W. H. Press, B. P. Flannery, S. A. Teukolsky, and W. T. Vetterling. In *Numerical Recipes*, chapter 11. Cambridge University Press, Cambridge, 1986. (http://www.library.cornell.edu/nr/bookfpdf.html).

[10] W. H. Press, B. P. Flannery, S. A. Teukolsky, and W. T. Vetterling. In *Numerical Recipes*, chapter 10. Cambridge University Press, Cambridge, 1986. (http://www.library.cornell.edu/nr/bookfpdf/f10-6.pdf).

[11] http://www-unix.mcs.anl.gov/mpi/,http://www-unix.mcs.anl.gov/mpi/tutorial/gropp/talk.html.

[12] I. Yamazaki, T. Murao, T. Yamanaka, and K. Yoshihara. *Faraday Discuss. Chem. Soc.*, 75:395, 1983.

[13] K. K. Innes, I. G. Ross, and W. R. Moonaw. *J. Mol. Spectrosc.*, 32:492, 1988.

[14] H. Köppel, W. Domcke, and L. S. Cederbaum. *Adv. Chem. Phys.*, 57:59–245, 1984.

[15] A. Raab, G. A. Worth, H. D. Meyer, and L. S. Cederbaum. *J. Chem. Phys.*, 110:936–946, 1999.

[16] G. Stock, C. Woywood, W. Domcke, T. Swinney, and B. S. Hudson. *J. Chem. Phys.*, 103:6851, 1995.

[17] M. Thoss, W. H. Miller, and G. Stock. *J. Chem. Phys.*, 112:10282–10292, 2000.

[18] M. Ben-Nun and T. J. Martinez. page 439. Wiley, New York, 2002.

[19] C. Coletti and G. D. Billing. *Chem. Phys. Lett.*, 368:289–298, 2003.

[20] D. V. Shalashilin and M. S. Child. *J. Chem. Phys.*, 121:3563–3568, 2004.

[21] C. Woywood, W. Domcke, A. L. Sobolewski, and H. J. Werner. *J. Chem. Phys.*, 100:1400, 1994.

[22] R.P. Feynman. In *Statistical Mechanics*. Benjamin, Reading, 1972.

[23] V. Guallar, V. S. Batista, and W. H. Miller. *J. Chem. Phys.*, 113:9510, 2000.

[24] V. Guallar, V. S. Batista, and W. H. Miller. *J. Chem. Phys.*, 110:9922, 1999.

[25] M. Petkovic and O. Kuhn. *J. Phys. Chem. A*, 107:8458, 2003.

[26] J.H. Shao and N. Makri. *J. Phys. Chem. A*, 103:7753, 1999.

[27] E. Jezek and N. Makri. *J. Phys. Chem. A*, 105:2851, 2001.

[28] N. Makri and W.H. Miller. *J. Chem. Phys.*, 116:9207, 2002.